Solar thermochemical energy storage in elemental sulphur: Design, development and construction of a lab-scale sulphuric acid splitting reactor powered by hot ceramic particles

Vamshi Krishna Thanda, Dennis Thomey, Lutz Mevißen, et al.

View Online

Export Citation

ARTICLES YOU MAY BE INTERESTED IN

Solar Thermochemical Energy Storage in Elemental Sulphur: Design, Development and Construction of a Lab-scale Sulphuric Acid Splitting Reactor Powered by Hot Ceramic Particles

Vamshi Krishna Thanda[1,a)], Dennis Thomey[1,b)], Lutz Mevißen[2,c)],
Hiroki Noguchi[3,d)], Christos Agrafiotis[1,e)], Martin Roeb[1,f)], Christian Sattler[1,g)]

[1]*German Aerospace Center (DLR), Linder Hoehe, 51147 Cologne, Germany*
[2]*RWE Generation SE, Ehinger Str. 200, 47259 Duisburg, Germany*
[3]*Japan Atomic Energy Agency, 4002 Narita-cho, Oarai-Machi, 311-1393, Japan*

[a)]Corresponding author: Vamshi.Thanda@dlr.de
[b)]Dennis.Thomey@dlr.de
[c)]lutz.mevissen@rwe.com
[d)]Noguchi.Hiroki@jaea.go.jo
[e)]Christos.Agrafiotis@dlr.de
[f)]Martin.Roeb@dlr.de
[g)]Christian.Sattler@dlr.de

Abstract. A proof of concept sulphuric acid splitting/decomposition prototype driven by hot bauxite particles is designed and developed. The lab-scale test reactor is a novel counter-current flow shell-and-tube heat exchanger with particles on the shell side and sulphuric acid on the tube side with mass flow rates of 10 kg/h and 2 kg/h, respectively. A one-dimensional heat transfer model was developed based on correlations of the flow boiling heat transfer coefficient and particle bed heat transfer coefficient for sizing the shell-and-tube heat exchanger. A detailed study was carried out in order to choose suitable materials especially in the sulphuric acid inlet and evaporation section. A new concept of an electrically heated, continuously operated particle heating system was designed and developed to provide the splitting reactor with hot particles. Different cases were studied using a finite element method (FEM) analysis to qualify the particle heater and examine its thermo-mechanical stability.

INTRODUCTION

Since the start of Industrialisation from 1750's, the CO_2 emissions has been increased to 5 billion tons per year by the mid of the 20th century. In the last decades, the energy demand has been growing exponentially due to modern development [1] and this upsurge in energy demand lead to global CO_2 emissions up to 35 billion tons per year. Alternative energy sources are one of the promising solutions to mitigate the global CO_2 emissions and thus global warming. Moreover, the new coal phase-out [2] is an immediate call for sustainable energy sources. Concentrated solar technologies are a potential solution to meet the aforesaid demand but the interrupted availability of solar radiation limits their application. This challenge can be overseen by storing the solar energy in energy carriers. Hydrogen is one of the bright options to store solar energy in its chemical bond potential. It can be produced from water using thermal water splitting, thermochemical cycles and electrolysis integrated with solar energy. Thermal water splitting cycles requires high temperatures (>2000 °C) whereas in thermochemical cycles the temperatures needed are lower (1400-1600 °C for redox cycles and <1000 °C for sulphur cycles) [3]. In contrast, conventional water electrolysis can be carried out at temperatures <100 °C, however, the required production of electricity results in lower

overall efficiency than the aforementioned thermal processes [4]. Besides hydrogen, sulphur is a promising option to store solar energy in its chemical bonds because of its high energy density. It can be easily transported in both solid and liquid state using various means of transportation without risk and minimum heat loss. A sulphur based thermochemical energy storage cycle was proposed by General Atomics [5, 6] as shown in **FIGURE 1a**, where the stored heat can be retrieved at a temperature higher than that of original heat input.
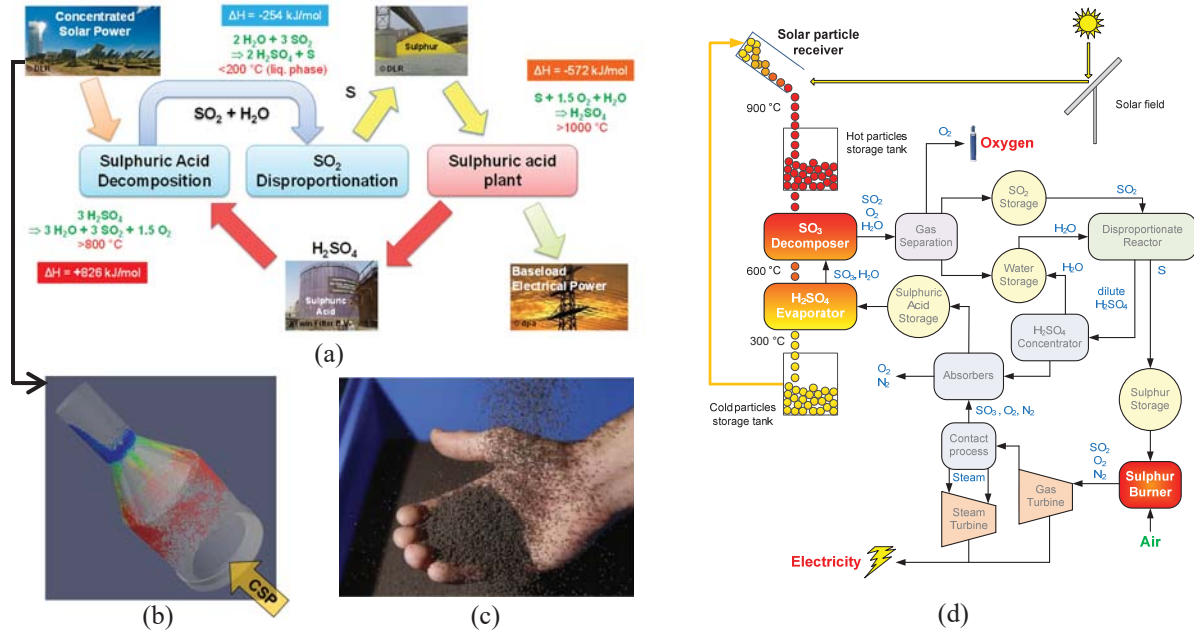

FIGURE 1. a) Solid sulphur cycle, b) Centrifugal particle receiver (CentRec), c) Bauxite particles, d) PEGASUS process cycle

Sulphuric acid decomposition is the prime step in all sulphur based thermochemical cycles [7]. DLR has successfully developed and tested directly irradiated solar receiver-reactors for sulphuric acid splitting process in different EU projects namely, HYTHEC [8], HycycleS [9] and SOL2HY2 [10]. Currently, DLR is investigating a novel thermochemical cycle in which the solid sulphur cycle (Figure 1a) is combined with DLR´s next generation particle receiver (**FIGURE 1b**) within the framework of the European research project PEGASUS. The bauxite particles (**FIGURE 1c**) are heated in the centrifugal particle receiver CentRec [11] with the help of solar irradiation and the hot particles are fed into the sulphuric acid splitting reactor. The heat energy of the particles is used to evaporate sulphuric acid to SO_3 which subsequently is decomposed into SO_2 with the help of a catalyst (e.g. Fe_2O_3) at a temperature above 800 °C. The produced SO_2 is mixed with water and converted into sulphur and sulphuric acid in a disproportionation reactor. The sulphur can be combusted with air in conventional contact sulphuric acid plants achieving temperatures >1000 °C suitable for the operation of a gas turbine [12] to generate baseload electricity (**FIGURE 1d**).

LAB SCALE SULPHURIC ACID SPLITTING REACTOR

One of the objectives in the project PEGASUS is to investigate a lab scale particle heated reactor test setup for sulphuric acid splitting as a proof of concept. The hot particles required to drive the process are heated using an electrical particle heater because solar heated particles are not available for the initial lab scale test. The particles which are electrically heated up to 900 °C acts as heat transfer medium and move downwards on the shell side while the sulphuric acid flows upward inside acid resistant tubes as shown in **FIGURE 2a**. The particles heat is utilized to evaporate and decompose the sulphuric acid into SO_2, H_2O and O_2. The particle flow is controlled with the help of a screw feeder which is connected at the bottom of the reactor and further conveying the particles at 300 °C to a particle collector for storage as shown in **FIGURE 2b**. The SO_2 gas produced is analysed by ultraviolet-visible (UV-Vis) spectrometry and finally the off gases are neutralised inside a scrubber.
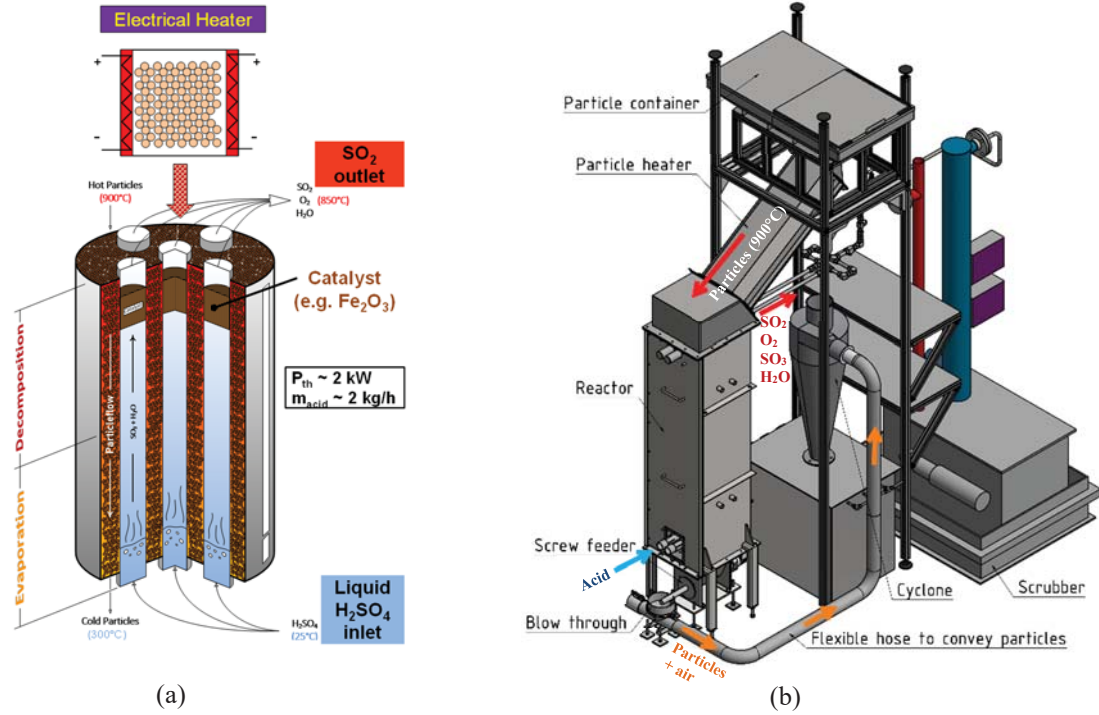
FIGURE 2. Particles driven sulphuric acid splitting reactor a) Concept development; b) CAD model of lab-scale test setup

Development of Particle Heater

The prime requirement of the particle heater is to heat the bulk to at least 850 °C and also to maintain the core temperature of the bulk as uniform as possible. The commercial heaters and ovens are limited to small particle volumes and are less flexible to integrate into the aforesaid test setup. Therefore, a new particle heater [13] was developed for this application as shown in **FIGURE 3a**. The particle heating system consists of a particle container (with maximum 100 liters volume) to store the cold particles, heater tube with 1000 °C heating cables wrapped around it and encapsulated with insulation and reactor interface. The one-meter heater tube is made out of high temperature stainless steel (1.4841) because this steel exhibits good mechanical properties at higher temperatures compared to other stainless steels [14]. Moreover, it is mainly used in the field of industrial furnaces. The heater tube has six sections as shown in **FIGURE 3b**. Section 1 and 6 are connected to the particle container and reactor, respectively, whereas sections 2 to 5 are actively heated. The repose angle of bauxite particles is 35°. Therefore, the heater tube is designed with this angle to the horizontal ensuring free flow of particles.

A large number of analytical equations for computing the transient heat conduction are well established for geometrically simple and static bodies. A double-side heated plate with constant surface temperature is used to develop a 1-D model according to Carslaw and Martin [15, 16] in which the time dependent temperature field $T(r, t)$ of a stagnant incompressible medium can be calculated using the first law of thermodynamics and Fourier's law of heat conduction. In this model, the Biot number is set to infinity as the temperatures of the surface and the surroundings are assumed to be identical. The core temperature $\theta_{X=0}$ as a function of normalized distance from the centre of symmetry X and Fourier number Fo ($\theta = \theta(X, Fo)$) can be calculated from the following equation:

$$\theta_{X=0} = \frac{2}{\pi} * \sum_{k=1}^{\infty} \frac{(-1)^{k+1}}{k - \frac{1}{2}} * e^{-\left(k - \frac{1}{2}\right)^2 \pi^2 Fo} \tag{1}$$

The thermal conductivity of the bulk is calculated from the unit cell model according to Zehner/Bauer/Schlünder [17] and the heat capacity of the bulk is calculated using a fourth-degree polynomial [18]. The heat transfer from a heated wall to a stagnant particle bed is explained by Schlünder and Tsotas (also named penetration model) [19]. According to this model, the overall heat transfer coefficient from the wall to the bulk is a series of two thermal resistances as formulated below:

$$\frac{1}{\alpha_{tot}} = \frac{1}{\alpha_{WS}} + \frac{1}{\alpha_{bed}} \qquad (2)$$

In the above equation, $1/\alpha_{WS}$ is the contact resistance from the wall to the first particle layer and $1/\alpha_{bed}$ is the heat penetration resistance inside the interior of the bulk.
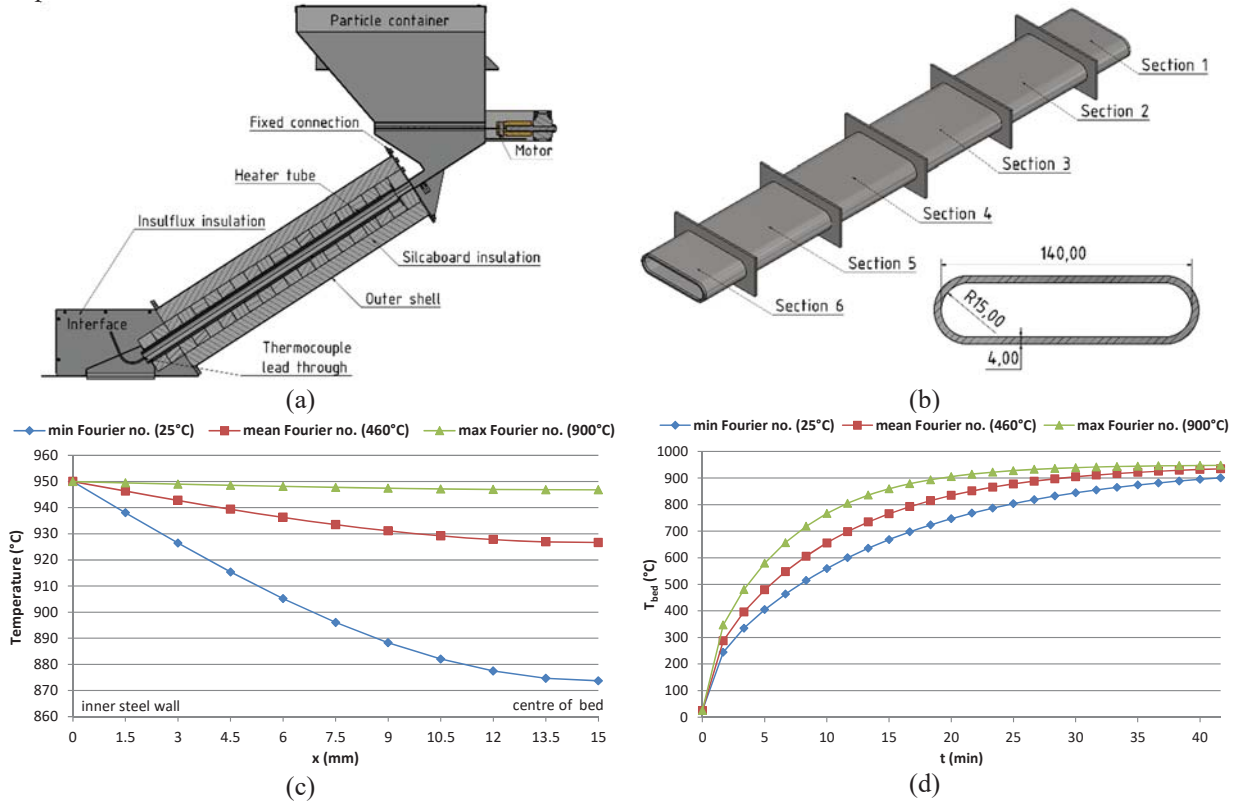

FIGURE 3. Particle heater a) Cross sectional view of particle heating system b) CAD model of the heater tube, c) Temperature curve of bulk as a function of the Fourier number, d) Mean temperature T_{bed} as a function of contact time t

The iterations of equation (1) results in three temperature curves for minimum (25 °C), mean (460 °C) and maximum (900 °C) Fourier number as depicted in **FIGURE 3c**. The graph shows that a minimum core temperature of 870 °C is reached although neglecting the increase of the heat capacity and the thermal conductivity of the bulk. **FIGURE 3d** shows the time required for the bulk to stay inside the heater tube to reach an average temperature of 850 °C for selected Fourier numbers. This graph depicts that the minimum contact time is approx. 22 minutes to reach a mean bulk temperature of 850 °C, if the mean Fourier number at temperature of 460 °C is considered. On the other hand, the contact time is at least 31 minutes for the Fourier number at temperature of 25 °C. The design flow rate of the particles is 10 kg/h i.e., the first layer of the bulk entering the active heating section of the heater tube (section 2) needs approximately 42 minutes to leave the heater tube (section 5) but the required overall minimum contact time of the particles for the selected heater design ranges between 22 and 31 minutes. Therefore, the results show that the 1-D transient model fulfils the prime requirement of the particle heater.

Finite Element Method Simulations of the Particle Heater

The mechanical integrity of the designed heater tube is investigated using thermal and mechanical FEM simulations. The thermal model is developed using the heating cables power supply of 2740 W, the overall heat transfer between the heater tube and the bulk $\alpha_{tot} = 22$ W/m^2 K and assuming the bulk temperature to increase constantly from 25 °C (section 1) to 900 °C (end of section 5). The constant surface temperature assumption is not suitable because the temperature profile between the inlet area (section 1) and the first heating area (section 2) of the heater tube are different as sections 2-5 are only heated. The temperature field corresponds very well to the

expectations, because the surface temperature of the heater tube is between 960 °C and 1015 °C as shown in **FIGURE 4a** and this is similar to the operating temperature of the electrical heating cables (1000 °C).
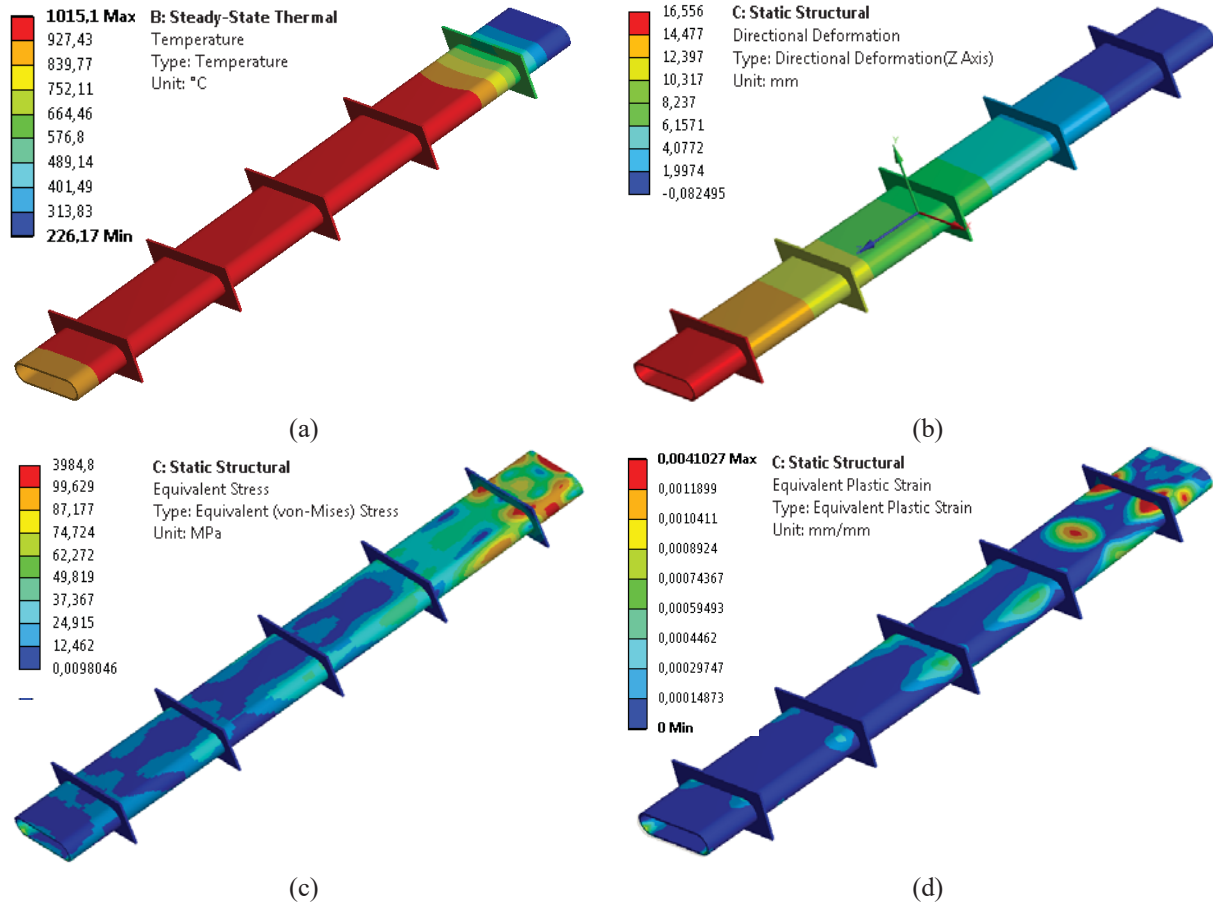

(a)

(b)

(c)

(d)

FIGURE 4. FEM simulation results a) Steady state thermal model, b) Thermal expansion of heater tube, c) Equivalent stress for mechanical-elastic analysis, d) Equivalent plastic strain for mechanical-plastic analysis

In the static structural model, section 1 is fixed and section 6 (outlet section) is a slide joint. The expansion of the conveying tube is shown in **FIGURE 4b** by adding the temperature field of the thermal model to the static structural FEM model. The heater tube expands approx. 17 mm in Z-axis and the expansion is parallel to the increase in the temperature of the bulk. This movement was considered during design so that the heater tube can slide into the interface at the top of the reactor during hot operations. In the initial mechanical-elastic analysis, the plastic deformation is neglected i.e., the tube will return back to its original shape by the end of the load cycle. The properties of the tube and the weight of the total particle heater are included in this model. The average stress shown in **FIGURE 4c** is in between 30 – 40 MPa which is below the maximum permissible mechanical stress of 550 MPa of the tube material (1.4841) [14]. The high stress near section 1 is due to the mechanically rigid connection and the assumed completely welded contact surface of the tube and the ribs. In the subsequent mechanical-plastic analysis, the plastic deformation of the tube is investigated as the temperature of the heater tube exceeds 1000 °C. The creep strain limit of 10 MPa at 1000 hours was determined as the yield point. The deformation of the heater tube is shown in **FIGURE 4d**. The strain in section 1 is because the tube experiences a transition between unheated and heated section. However, the model converges with the condition that a combined thermal mechanical stress of 10 MPa is not allowed to be exceeded.

Hence, from the simulations it can be concluded that the particle heater will not fail during operation. Although mechanical and thermal stress locally exceeds the yield strength of the tube material, the mechanical-plastic analysis shows that the tube suffers a minimum permanent deformation. The plastic deformation can be minimized by adding a stable support structure to the particle heater and by reducing redundant welding seams.

Sizing of the Splitting Reactor

The sulphuric acid decomposition takes place in several steps which include physical and chemical processes and can be subdivided into following zones: heating of liquid acid, dehydration, evaporation of water followed by acid, converting H_2SO_4 to SO_3 and H_2O, superheating of gas mixture and finally splitting of SO_3 to SO_2 and O_2 [20, 21]. The modelling of the splitting reactor was carried out in two sections, namely evaporator and decomposer. The evaporator deals with conversion of the acid into SO_3 while the further reduction to SO_2 takes place in the decomposer. Initially, the heat required for both evaporator and decomposer is calculated for different sulphuric acid mass flow rates. The heat required for evaporation is twice that of the decomposer as shown in **FIGURE 5** because of the state of the fluid in the respective sections. From the energy balance, a 1.8 kg/h flow rate of sulphuric acid and 10 kg/h particle flow results in a temperature drop of the particles from 900 °C to approx. 300 °C. The particle flow rate could be further reduced to lessen the particle outlet temperature for a 2 kW reactor but this would adversely affect the tube length. Therefore, the flow rates of the process fluid and the particles are considered as stated above.
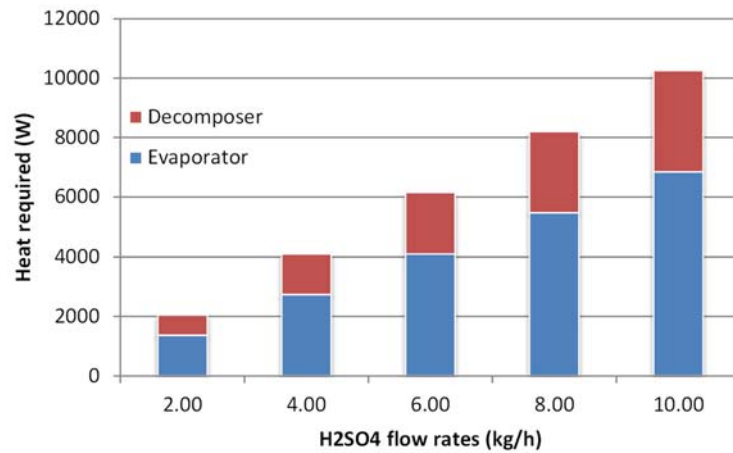

FIGURE 5. Heat required for evaporator and decomposer (75 wt% sulphuric acid)

Initially, there were ideas to separate the evaporator and decomposer sections physically, but in the later stages of development they are integrated into one system to make the construction simpler in such a way that the evaporation section, decomposition section including catalyst section is in a single tube as shown in **FIGURE 6a**.
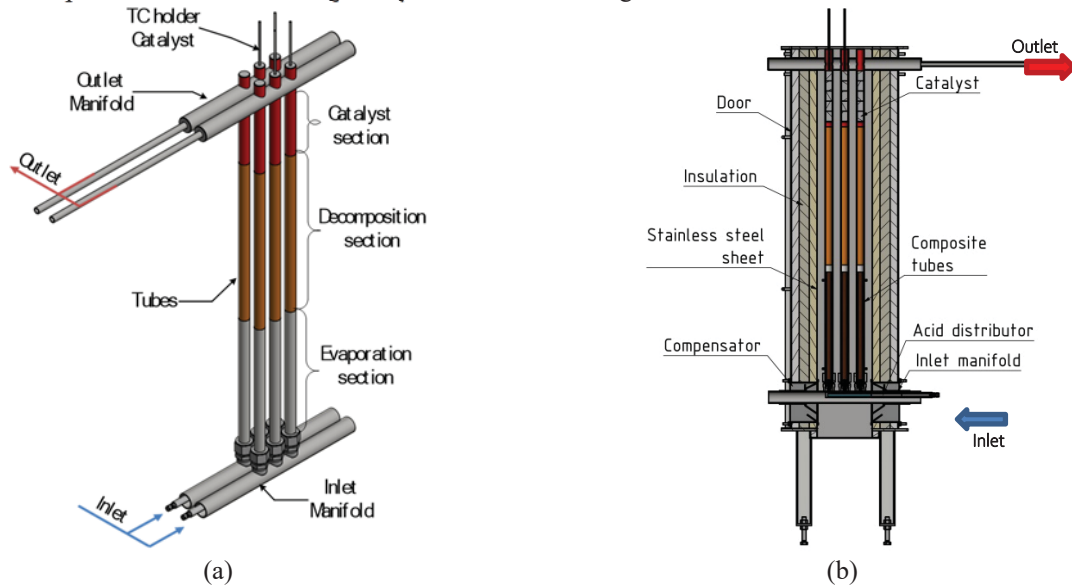

FIGURE 6. 3D-model of the reactor components, a) reactor tubes, b) cross sectional view of the splitting reactor with tubes

There are two sets of tube bundles and each tube bundle has three tubes. The tubes are connected to inlet and outlet manifold at the bottom and the top, respectively. The inlet manifold is inserted into the compensators which are installed on the reactor walls while the outlet manifold is fixed at the top of the reactor as shown in **FIGURE 6b**. The inlet manifold has an acid distributor made out of Hastelloy C276 to minimize the effect of corrosion. The tube material choices in the evaporation section are very limited because of the high corrosivity of boiling sulphuric acid [21]. Therefore, composite tubes (OD 32 mm stainless steel tube with OD 28 mm SiC tube as in-liner) are created for this section to avoid direct contact of the fluid with metal parts during phase change.

Normally, thermodynamic sizing refers to determination of the heat transfer area of the heat exchanger and the commonly used method is the F-correction factor method or log-mean temperature difference method (LMTD) [22] as shown in Equation 3. This method is used to develop a 1-D thermodynamic model considering that the sulphuric acid splitting reactor behaves similar to a counter-current flow shell and tube heat exchanger.

$$\dot{Q} = k * A * \Delta T_{lmtd} \tag{3}$$

ΔT_{lmtd} is the effective mean temperature difference, A is the heat transfer area and k is the overall heat transfer coefficient. The overall heat transfer coefficient is calculated from Equation 4 where α_{tube} is the heat transfer coefficient on the tube side and α_{tot} is the heat transfer coefficient on the particle side. The α_{tot} can be calculated using the penetration model from Equation 2.

$$\frac{1}{k} = \frac{1}{\alpha_{tube} * d_{ri}} + \frac{\ln\left(\frac{d_{ra}}{d_{ri}}\right)}{2 * \lambda_{tube}} + \frac{1}{\alpha_{tot} * d_{ra}} \tag{4}$$

Within the **evaporator** section [23] there are three different heat transfer coefficients on the tube side because of the phase change, namely, liquid (α_{LO} in zone 1), flow boiling (α_{fb} in zone 2, 3) and gas (α_{GO} in zone 4) heat transfer coefficients as shown in **FIGURE 7a**. The algorithm of the evaporator model is shown in **FIGURE 7b**. The heat exchangers in which the subcooled liquid is boiled and completely evaporated and the gas is super-heated are regarded as coupled systems. They are treated as separate heat exchangers and the heat transfer areas obtained from each unit are summed up to obtain the total heat transfer area of the complete system. Therefore, the overall heat transfer coefficients are determined separately for each zone from heat transfer coefficients in the respective zone.
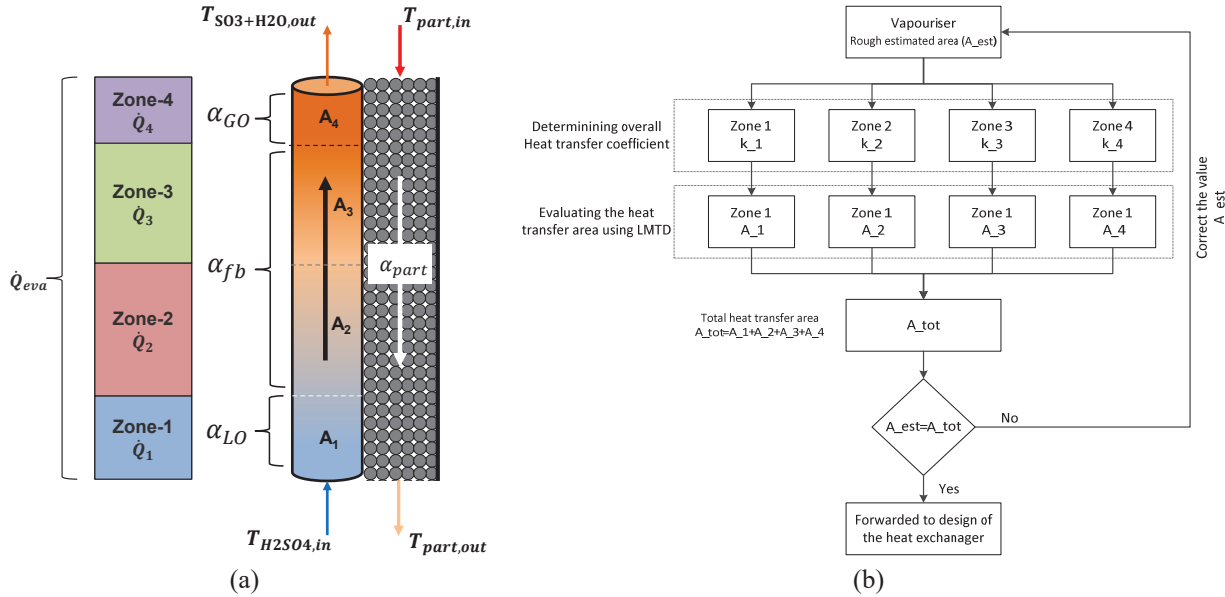

FIGURE 7. Evaporator model, a) 1-D model for estimating the evaporator heat transfer area, b) algorithm of evaporator model

The flow boiling heat transfer coefficient is calculated according to Steiner-Taborek asymptotic model correlations [24] as shown in Equation 5 where α_{nbf} is nucleate boiling component and α_{cb} convective flow boiling component.

$$\alpha_{fb} = \left[(\alpha_{nbf})^3 + (\alpha_{cb})^3\right]^{\frac{1}{3}} \tag{5}$$

The flow boiling heat transfer coefficient is higher than the liquid phase and gas phase heat transfer coefficients. **FIGURE 8a** describes the effect of increasing flow boiling heat transfer coefficient on the overall heat transfer coefficient for a constant particle heat transfer coefficient. The increase in flow boiling heat transfer coefficient did

not affect the overall heat transfer coefficient because of the poor heat transfer coefficient on the particle side (α_{tot} $\ll \alpha_{fb}$). Therefore, the particle heat transfer coefficient is a sensitive factor to improve the overall heat transfer coefficient.
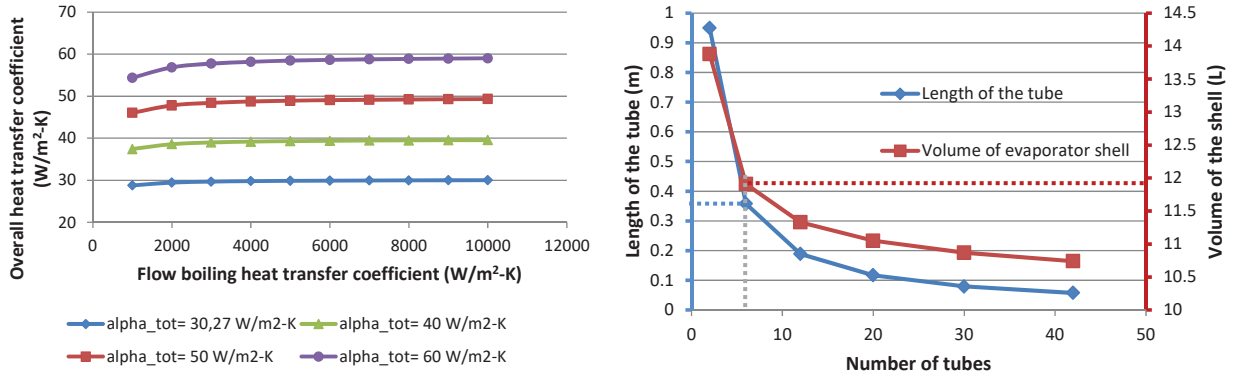

FIGURE 8. a) Effect of flow boiling heat transfer coefficient on overall heat transfer coefficient for different α_{part}, b) Sizing of the evaporator section for 10 kg/hr particle flow and 1.8 kg/h acid flow

The analysis in **FIGURE 8b** illustrates the sizing of the evaporator (for 10 kg/hr particle flow and 1.8 kg/h acid flow) including the shell volume due to the limited amount of particles in the particle heater. For a fixed tube diameter, the increase in tube length decreases the number of tubes with an increase in particle volume and vice versa. For a standard tube diameter of 32 mm and approx. 12 liters of shell volume, the tube length is 370 mm with a total of 6 tubes.

The **decomposer** contains the gas phase; hence, the sizing is carried out by determining the overall heat transfer coefficient from the particle side and gas phase heat transfer coefficients. A separate parametric study was performed for the decomposer similar to that of the evaporator but for two different particle mass flow rates, 10 kg/hr and 50 kg/hr as shown in **FIGURE 9a**. In this figure, the blue and red curve refers to 10 kg/hr and 50 kg/hr particle mass flow rate, respectively. The length of the tube and the shell volume is increased by approx. 4 times if the particle flow is increased by 5 times, i.e. 50 kg/hr. For 10 kg/hr particle flow, the shell volume increases at decreasing number of tubes in a similar way as for the evaporator section (cf. **FIGURE 8**). Therefore, the same numbers of tubes are chosen for both sections and this leads a tube length of 750 mm because of the limitations concerning the dimensions of the experimental test bench (1.0 x 0.6 x 1.9 m), the particle volume inside the particle container (maximum of 100 liters) and the experimental time which is set to 4 hours of chemical testing (with an additional 2+2 hours for start-up and shut-down).
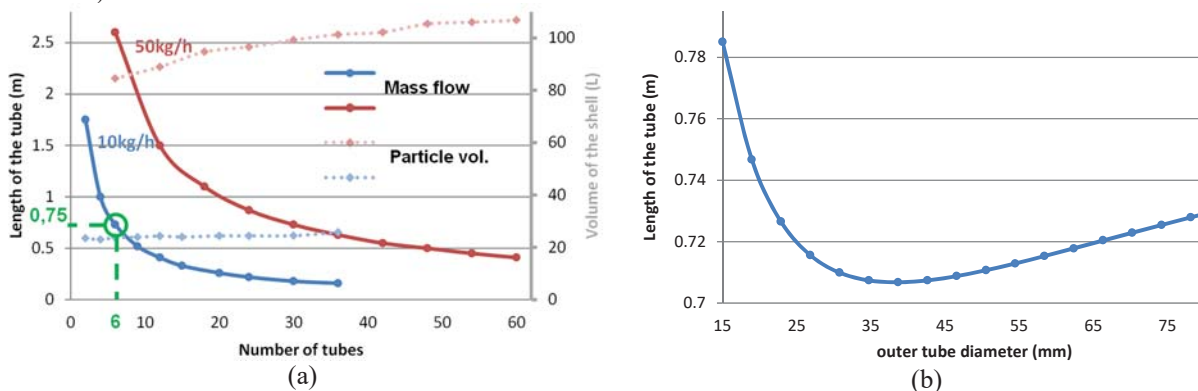

(a)   (b)

FIGURE 9. Decomposer, a) Sizing of the decomposer section, b) Optimum outer tube diameter

A parametric study was conducted on the tube arrangement with the length of the decomposer tube as a function of the tube diameter to identify the optimum tube diameter as shown in **FIGURE 9b**. Smaller tube diameters increase the heat transfer coefficient on the tube side, but decrease the heat transfer area and vice versa and the graph shows an

optimum value of about 35 mm; hence, 32 mm diameter is a good choice because it is readily available in the market in almost all grades of steels.

Compensator Development and Pre-testing

The thermal expansion of the tubes ($\Delta l = l_t * \alpha * \Delta t$, where Δl is the change in length, l_t is the initial length of the tube at ambient temperature, α is the linear coefficient of thermal expansion and ΔT the temperature change) is calculated to be 22.3 mm with a maximum design bulk temperature of 900 °C. A new expansion joint is developed to compensate the linear expansion of the tube because the commercially available compensators are found to be not suitable in the given particle environment.
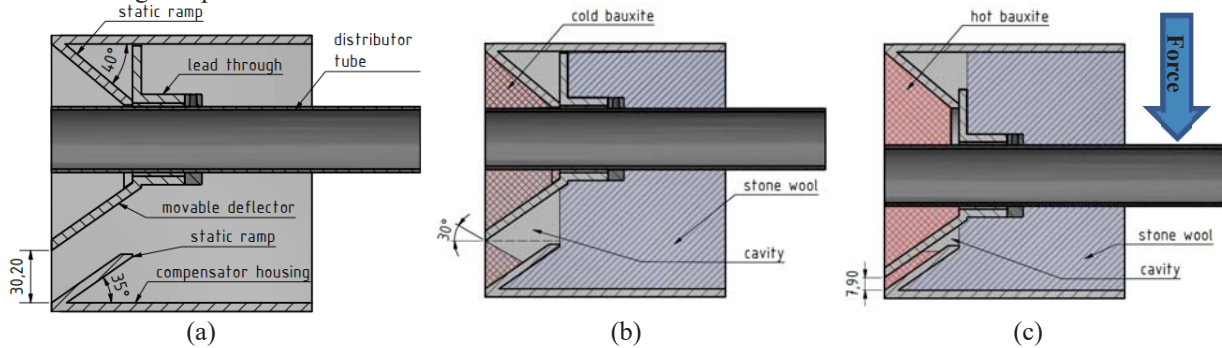

FIGURE 10. Compensator concept development a) Compensator cross section view, b) Compensator at zeroth position, c) Compensator during operation

The main challenges of the compensator in this application are that the flow behaviour of the particles should neither be influenced nor be clogged and the reactor shell should be leak proof. Therefore, the simple steam boiler construction principle is used where the outlet manifold is fixed and the inlet manifold expands linearly. Moreover, the compensators should be installed directly inside the reactor shell to avoid particles leakage.

The cross section view of the compensator is shown in **FIGURE 10a**. The complete design consists of two main components, namely compensator housing and movable deflector. The components of the compensator are provided with a static ramp (35° and 40°) because of the angle of repose of bauxite particles. One end of the inlet manifolds is inserted into the lead through of the movable deflector.

The position of the compensator when filled with cold particles is shown in **FIGURE 10b**. If the cold particles are slowly replaced with hot particles, the tubes expand linearly by shifting the movable deflector downwards and this movement will push the particles inside the cavity into the reactor. In addition, the cavity can accommodate the full amount of particles without pushing the particles into the reactor even under compression.

FIGURE 11. Pretesting of 3-D printed plastic compensator a) compensator in operation, b) deflection measurement

Since the above mentioned compensator concept was completely custom made, a 1:1 scale 3-D printed compensator was manufactured from plastic to pretest the functionality, flowability and tightness under ambient conditions. Besides exact dimensions, the compensator is equipped with a couple of observation windows to track the

repose angle and the particle distribution inside the cavity as shown in **FIGURE 11a**. When the pretest setup is filled with cold particles, the particles form a repose angle of approximately 30° inside the cavity.
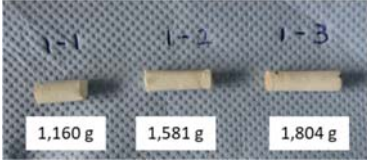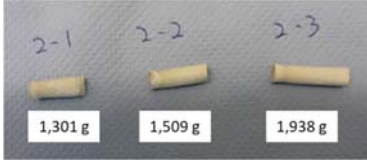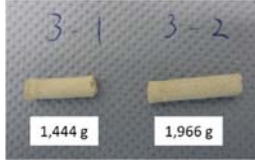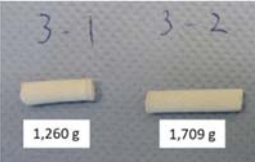
Extra weights are placed on the inlet manifold to simulate the force exerted during thermal expansion as shown in **FIGURE 11a**. During the experiment, the force causes the deflector to move downwards as the particle flow is initiated and the deflection is measured as shown in **FIGURE 11b**. The results of the pretest fulfils the challenges that the compensator can absorb an axial movement of more than 25 mm with an average mass flow of 25.2 kg/h and an extra weight of 11.6 kg with almost no leakage of particles.

Corrosion Resistant Material Testing

The corrosion resistant materials available for sulphuric acid at higher temperatures (>100 °C) are very limited [21]. The commercially available inorganic silicate-based bedding material POTSIL was selected and pretested for application in the evaporator inlet manifold. POTSIL is provided in a two component format: a potassium silicate solution and a catalysed filler powder. The main aim of the material qualification is to confirm the acid resistance of POTSIL when it is used as a hardening agent in the liquid acid inlet section.

The cylindrical test samples are immersed in 75 wt.% sulphuric acid solution at different temperatures for different immersion time as shown in **TABLE 1**. The weight of the test samples is measured before and after the test (samples are slightly washed with water and dried after the chemical treatment before weighing). Three tests were conducted with three different cases as shown in **TABLE 1**.

TABLE 1. Corrosion test

Test case 1: 75 wt. % sulphuric acid Temperature – 100 °C Immersion time – 3 hours	Test case 2: 75 wt.% sulphuric acid Temperature – 120 °C Immersion time – 3 hours	Test case 3: 75 wt.% sulphuric acid Temperature – 100 °C Immersion time – 20 hours
 1,160 g · 1,581 g · 1,804 g Before test (case 1 , sample 1,2,3)	 1,301 g · 1,509 g · 1,938 g Before test (case 2 – sample 1,2,3)	 1,444 g · 1,966 g Before test (case 3 – sample 1,2,3)
 1,027 g · 1,396 g · 1,578 g After test	 1,160 g · 1,332 g · 1,701 g After test	 1,260 g · 1,709 g After test

The average weight loss of samples in test case 1, case 2 and case 3 are 0.060, 0.061 and 0.011 gram/hour, respectively. The corrosion rate is calculated per year with respect to immersion time and plotted in a graph as shown in **FIGURE 12**.
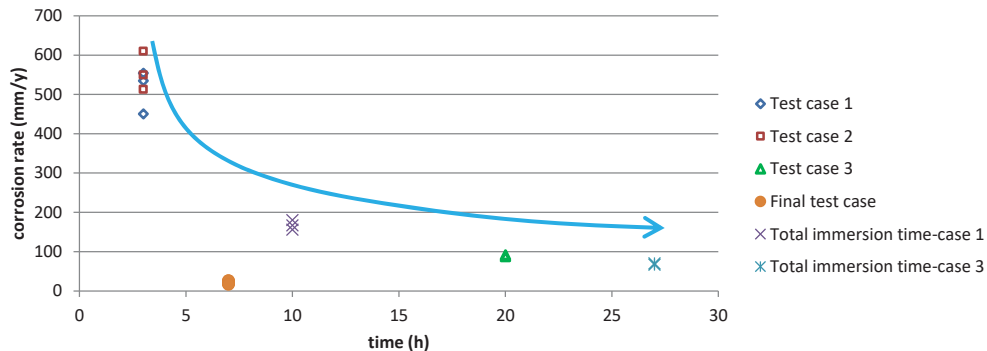

FIGURE 12. POTSIL test results

The loss of weight is relatively low in case 3 compared to case 1 and 2, i.e. the corrosion rate is decreasing significantly for the longer immersion time like in test case 3 because of release of dissolvable components during the tests from the samples. If the immersion time is longer, the released components are dissolved in the acid and thereafter the corrosion rate of the samples is significantly reduced.

The after-test samples from test case 1 and 3 as shown in **TABLE 1** were reused in the final test case where the immersion time is set to another 7 hours and the temperature to 100 °C. The corrosion rate of the reused samples (final test case) is between 18-26 mm/y because these samples are already free from dissolved components but if the total immersion time of the test case 1 and 3 samples including the previous test cases 1 and 2 are considered, then the corrosion rate is further reduced as shown in **FIGURE 12**. This pretest concludes that POTSIL exhibits good corrosion resistance when it is free from dissolvable elements. Therefore, POTSIL was successfully qualified to be used in the considered sulphuric acid application considering preparation according to manufacturer recommendations and avoiding contact with water.

CONCLUSIONS

A new design of particle driven sulphuric acid splitting reactor was developed. A 1-dimensional lumped model was developed for the evaporator and decomposer section of the reactor. The main goal is to estimate the heat transfer area (sizing). The model includes calculations for estimating the overall heat transfer coefficients considering heat transfer on the fluid and particle side. An assumption of dividing the complete evaporator into different zones (liquid, flow boiling, and gas phase) was made and the overall heat transfer coefficient in each zone was calculated. Finally, with these results the individual heat transfer area for the different zones was calculated applying the logarithmic mean temperature difference (LMTD) method. As a result, for a particle flow rate of 10 kg/hr and acid flow rate of 1.8 kg/hr, the length of the tubes in the evaporation section is 370 mm with 6 tubes in a square pitch tube layout configuration. A composite tube (stainless steel tube with a SiC in-liner) was designed and manufactured to minimize corrosion in this evaporator section. The decomposer model calculated a tube length of 750 mm for superheating the sulphuric acid vapours to >800 °C with subsequent catalytic formation of SO_2. The parametric study of tube arrangements concluded that the optimum diameter of the tube of 35 mm is close to the selected 32 mm commercial tube.

For lab-scale testing of this prototype an electrical particle heating system was developed. A detailed thermodynamic model of the heater tube was programmed in order to determine the electrical power requirement and the thermal parameters of the heater. The calculated electrical power needed to raise the particle temperature from 25°C to 900°C for the flow rate of 10kg/h is 2730 W. The model also shows that the new particle heater meets the requirement of a minimum bulk temperature of 850°C for the selected geometry and thermal properties of the bauxite particles with a calculated minimum core temperature of the particle bulk of 870°C for an operating temperature of the heating cables of 950 °C. The confirmation the mechanical strength of the new heater design was performed using an FEM analysis. The results show that the heater withstands an operating temperature of 1000 °C with an additional load of 150 kg (insulation, etc.) without failure.

In order to avoid mechanical stresses due to thermal expansion, a compensator for particles application was designed with deflector plates that allow the particles to flow back into the reactor chamber. The concept was pretested with a 3-D printed plastic model to check the functionality proving that the new compensator design is suitable to accommodate the maximum possible thermal linear expansions of 22.3 mm of the reactor tubes. Furthermore, the silicate based commercial bedding material POTSIL was pretested for corrosion resistance qualifying it for use as a sealing material inside the acid inlet manifold.

All the components are being manufactured and will be assembled together in a research lab at DLR Juelich. After initial operations, the system will undergo a systematic proof of concept testing procedure to examine the thermal and chemical performance of the particle reactor and analyse the suitability of the selected materials. Finally, the set-up will be transferred to the large-scale solar simulator, Synlight at DLR Juelich for combined demo operation with a 150 kW centrifugal particle receiver prototype.

ACKNOWLEDGMENTS

REFERENCES

1. R. Lindsey, "Climate Change: Atmospheric Carbon Dioxide," 14 August 2020. [Online]. Available: https://www.climate.gov/news-features/understanding-climate/climate-change-atmospheric-carbon-dioxide.

2. I. E. A. (IEA), "Germany 2020 Energy Policy Review," International Energy Agency (IEA), France, 2020.

3. M. Roeb, N. Monnerie, A. Houaijia, D. Thomey and C. Sattler, "Solar Thermal Water Splitting," in *Renewable Hydrogen Technologies*, Amsterdam, Elsevier, 2013, pp. 63-86.

4. N. P. Siegel, J. E. Miller, I. Ermanoski, R. B. Diver and E. B. Stechel, "Factors Affecting the Efficiency of Solar Driven Metal Oxide Thermochemical Cycles," *Industrial & Engineering Chemistry Research,* vol. 52, no. 9, pp. 3276-3286, 2013.

5. B. Wong, L. Brown, R. Buckingham, W. Swee, B. Russ and M. Gorensek, "Sulfur dioxide disproportionation for sulfur based thermochemical energy storage," *Solar energy,* vol. 118, p. 134–144, 2015.

6. J. H. Norman, "SULFURIC ACID-SULFUR HEAT STORAGE CYCLE". Patent US Patent No. 4,421,734, 20 December 1983.

7. C. Sattler, M. Roeb, C. Agrafiotis and D. Thomey, "Solar hydrogen production via sulphur based thermochemical water-splitting," *Solar Energy,* vol. 156, p. 30–47, 2017.

8. A. Noglik, M. Roeb, C. Sattler and R. Pitz-Paal, "Experimental study on sulfur trioxide decomposition in a volumetric solar receiver–reactor," *International Journal of Energy Research,* vol. 33, no. 9, pp. 799-812, 2009.

9. D. Thomey, L. d. Oliveira, J.-P. Säck, M. Roeb and C. Sattler, "Development and test of a solar reactor for decomposition of sulphuric acid in thermochemical hydrogen production," *International Journal of Hydrogen Energy,* vol. 37, no. 21, pp. 16615-16622, 2012.

10. J. L. Lapp, A. Guerra-Niehoff, S. Hans-Peter, D. Thomey, M. Roeb and C. Sattler, "Modeling of a Solar Receiver for Superheating Sulfuric Acid," *Journal of Solar Energy Engineering,* vol. 138, no. 4, p. 041013, 2016.

11. M. Ebert, L. Amsbeck, J. Rheinländer, B. Schlögl-Knothe, S. Schmitz, M. Sibum, R. Uhlig and R. Buck, "Operational experience of a centrifugal particle receiver prototype," in *AIP*, 2019.

12. H. R.T.C. and W. A.G., "Gas turbine topping for increased energy recovery in sulphuric acid manufacture," *Applied Energy,* vol. 3, no. 1, pp. 23-40, 1977.

13. M. Lutz, "Detailed engineering of a particle heated lab scale reactor for decomposition of sulphuric acid," Master Thesis, Köln, 2019.

14. thyssenkrupp Materials(UK) Ltd, "Material Data Sheet 1.4841," 06 2017. [Online]. Available: https://ucpcdn.thyssenkrupp.com/_legacy/UCPthyssenkruppBAMXUK/assets.files/material-data-sheets/stainless-steel/stainless-steel-1.4841.pdf. [Accessed 03 2021].

15. H. Martin, Transient conduction in stagnant media, 2 ed., Berlin: Springer-Verlag, 2010.

16. H. S. Carslaw, Mathematical theory of the conduction of heat in solids, 2 ed., London: Macmillan and Co., 1921, pp. 15-25.

17. E. Tsotsas, "Thermal Conductivity of packed beds," in *VDI Heat Atlas*, 2 ed., Berlin , Springer-Verlag, 2010, pp. 570-580.

18. M. A. Reichert, "Masterarbeit - Konzeptentwicklung und Konstruktion eines Direktkontakt-Wärmeübertragers für Keramikpartikel und atmosphärische Luft," 2014.

19. E. Tsotas, "Heat Transfer from a Wall to Stagnant and Mechanically Agitated Beds," in *VDI Heat Atlas*, 2 ed., Berlin, Springer-Verlag, 2010, pp. 1311-1326.

20. A. Noglik, "Entwicklung eines solaren Reaktors zur Schwefelsäurespaltung für die thermochemische Wasserstofferzeugung," Diss. RWTH Aachen University, 2008, Aachen, 2008.

21. K.-W. Eichenhofer, K. Huder, E. Winkler and K. H. Daum, "Schwefel und anorganische Schwefelverbindungen," in *Chemische Technik: Prozesse und Produkte. Band 3: Anorganische Grundstoffe, Zwischenprodukte.*, Wiley-VCH Verlag GmbH & Co. KGaA, 2005.

22. F. P. Incropera, Fundamentals of Heat and Mass Transfer, John Wiley & Sons, Inc., 2007.

23. V. K. Thanda, „Master Thesis - Thermochemical Production of Sulfur as Solar fuel: Design and development of moving bed heat exchanger for sulfuric acid evaporation heated by ceramic particles", Cologne, 2018.

24. D. Steiner and J. Taborek, "Flow Boiling Heat Transfer in Vertical Tubes Correlated by an Asymptotic Model," *Heat Transfer Engineering ,* vol. 13, no. 2, pp. 43-69, 1992.